

Development of Advanced Coatings for Laser Modifications Through Process and Materials Simulation

R. P. Martukanitz¹ S. S. Babu²

¹ *Applied Research Laboratory, Pennsylvania State University, State College, PA 16803*

² *Oak Ridge National Laboratory, Materials Joining Group, Oak Ridge, TN 37831-6096*

A simulation-based system is currently being constructed to aid in the development of advanced coating systems for laser cladding and surface alloying. The system employs loosely coupled material and process models that allow rapid determination of material compatibility over a wide range of processing conditions. The primary emphasis is on the development and identification of composite coatings for improved wear and corrosion resistance. The material model utilizes computational thermodynamics and kinetic analysis to establish phase stability and extent of diffusional reactions that may result from the thermal response of the material during virtual processing. The process model is used to develop accurate thermal histories associated with the laser surface modification process and provides critical input for the non-isothermal materials simulations. These techniques were utilized to design a laser surface modification experiment that utilized the addition of stainless steel alloy 431 and TiC produced using argon and argon and nitrogen shielding. The deposits representing alloy 431 and TiC powder produced in argon resulted in microstructures retaining some TiC particles and an increase in hardness when compared to deposits produced using only the 431 powder. Laser deposits representing alloy 431 and TiC powder produced with a mixture of argon and nitrogen shielding gas resulted in microstructures retaining some TiC particles, as well as fine precipitates of Ti(CN) formed during cooling and a further increase in hardness of the deposit.

INTRODUCTION

Laser surface modifications, in the form of cladding and alloying, are gaining widespread use because of their ability to provide high deposition rates, low thermal distortion, low base-metal dilution, low metallurgical degradation of the base material, and refined microstructures in the deposition due to high solidification rates. Because of these attributes, laser-based processing is considered a prime candidate for producing high wear resistant surfaces through the addition of hard particles, such as carbides, borides, or nitrides, and the formation of composite coatings. However, the ability of these two-phase systems to retain their advantageous structure during processing is extremely dependent upon the chemical stability and reaction kinetics of the material system.

The properties of a laser modified surface are developed through localized melting and solidification. The laser surface modification process alters the solidified microstructure by alloy-induced transformations, composite strengthening through

production of second-phase particles, or a combination of both. A variety of applications have been developed for the laser surface modification process. The most common uses are for improving resistance to corrosion, abrasion, erosion, oxidation, and wear. The properties of the modified surface depend on the microstructure that evolves during melting and cooling. One of the most common microstructural changes is the dissolution of primary phases, leading to precipitation of complex phases during melting and subsequent solidification [1]. For example, during laser surface modifications on nickel-based alloys with silicon carbide particles, the particles melt in the liquid pool, and during subsequent solidification, M_7C_3 carbides precipitate from the liquid [2]. Previous work has attempted to control the surface modified microstructure by adjusting the laser beam parameters and by changing the alloying additions through extensive experimental research [3, 4].

As a means to achieve additional wear resistance of surface depositions, recent research has been directed at adding constituents that alter the solidified

microstructure by alloy-induced transformations, developing a composite microstructures containing hard particles, or a combination of both [5-8]. Of particular interest is the addition and retention of hard particles, such as carbides, nitrides, and borides, into ferrous and non-ferrous alloys that impart high hardness and wear resistance on the surface while retaining the toughness of the substrate material.

As mentioned earlier, an important consideration in formulating composite coating systems involves the stability of the system during and immediately after processing. Hence, this research entailed the development of advanced processing and simulation techniques for predicting and selecting materials and appropriate processing parameters that would result in the retention of the hard particle reinforcement. The development of thermo-kinetic analyses, coupled with development of advanced processing techniques, offer a cost-effective method for designing and implementing composite coating systems that may have a vast ramification to industry. The approached utilized during this investigation is shown graphically in Figure 1.

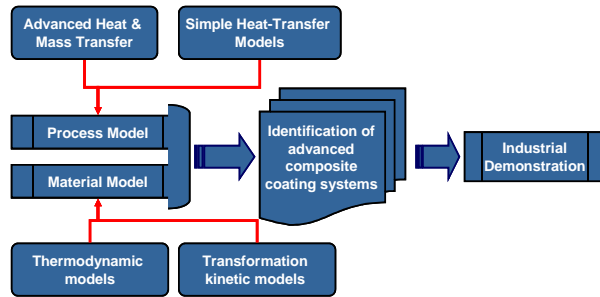


FIGURE 1. Relationships between process and materials models for development of advanced composite coatings.

PROCESS MODEL

The laser surface modification process is typified by a concentrated energy input from a laser beam to a metal powder either residing on the surface of a metal substrate, added to the beam and material interaction region, or added coaxially to the laser beam. The powder is melted along with a small amount of substrate material, metallurgically bonding the powder layer to the substrate, thus creating a new surface. An illustration of the laser surface modification process showing the introduction of energy by the beam, Q_{in} , conduction through the substrate, and surface heat losses, Q_{out} , is illustrated in Figure 2. The translation

of the beam over the substrate causes rapid heating of the coating and substrate material, followed by relatively rapid cooling. The study of heat flow within this system is essential to predicting useful process parameters, as well as for predicting the formation of phases and structures within the coating and microstructural changes due to the resulting thermal treatment of the substrate.

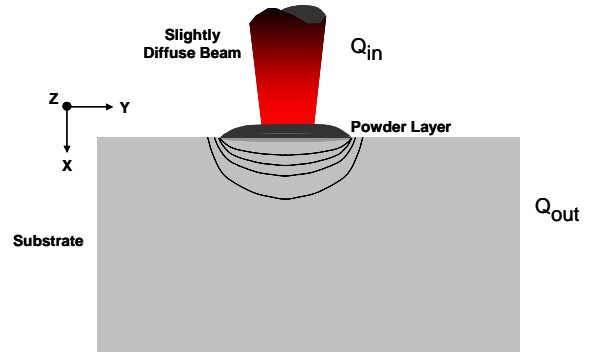


FIGURE 2. Schematic of the laser surface modification process showing heat input to the substrate, conduction through the substrate, and losses from the surface.

The energy balance for such a system may be represented in three-dimensional form as:

$$\rho C_p(T) \frac{\partial T}{\partial t} = \frac{\partial}{\partial x} \left[k_x(T) \frac{\partial T}{\partial x} \right] + \frac{\partial}{\partial y} \left[k_y(T) \frac{\partial T}{\partial y} \right] + \frac{\partial}{\partial z} \left[k_z(T) \frac{\partial T}{\partial z} \right] + Q_{in} - Q_{out} \quad (1)$$

where k is the thermal conductivity of the various material components (powder and substrate), ρ is the material density, C_p is specific heat, T is temperature, and x , y , and z are spatial coordinates. As described above, Q_{in} represents the introduction of energy by the beam and conduction through the substrate and Q_{out} accounts for convective and radiative heat losses at the surfaces. The above partial differential equation can be approximated by spatial discretization and employing the Euler method to solve through an explicit numerical technique [9].

Thermal properties are considered to be independent of temperature. However, during changes in phase, certain properties are approximated to change linearly with temperature. Upon melting of the powder, the powder is consolidated, thus, altering its thermal conductivity and density. The specific heats

of both the powder and the substrate also change during melting to account for latent heat of fusion. The conductivity after melting is equal to the theoretical conductivity of the solid material, k_{solid} , but the conductivity of the loose powder, k_{powder} , is calculated by viewing the powder as a bed of solid particles having gas-filled asperities [10]:

$$\frac{k_{\text{powder}}}{k_{\text{air}}} = V_s N_c * 2 \ln \left(\frac{k_{\text{solid}}}{k_{\text{gas}}} \right) - 11 \quad (2)$$

where N_c is the coordination number of the powder particles, V_s is the volume fraction of the solid particles, and k_{gas} is the conductivity of the gas asperities and is assumed to be air. The density behaves in the same manner as the thermal conductivity for the powder, showing a linear increase from the apparent density of the loose powder to the theoretical solid density of the solid material. The latent heat of fusion is treated within the function defining specific heat.

MATERIALS MODEL

The ability of a hard particle to be retained within the laser melt pool is governed by the initial size of the particles, the thermal cycle that the particles experience, the thermodynamic stability of the particles within the molten pool, and the rate at which dilution may occur. The model recently presented by Babu et al. [11], which utilizes ThermoCalc® software, may account for these complexities. In this approach, the composition of the substrate is initially used to determine thermodynamic equilibrium between the molten pool and the various possible reaction products. The phase having the greatest stability is based on the magnitude of the driving force for the reaction, i.e. the greatest change in free energy associated with a particular reaction. Subsequent kinetic analysis is based on the most suitable phase representing the rate-controlling process.

The stability of a phase is governed by its free energy, which is a function of temperature and its constitution. A generic description of free energy of a solid-solution phase, ϕ , G^ϕ , is given by the following equation [12]:

$$G^\phi = G_o^\phi + G_{\text{ideal-mix}}^\phi + G_{\text{excess-mix}}^\phi \quad (3)$$

where G_o^ϕ is the free energy contribution from pure components in that phase, $G_{\text{ideal-mix}}^\phi$ is the

contribution from ideal mixing, and $G_{\text{excess-mix}}^\phi$ is the contribution due to non-ideal interactions between the components. With the description of this G^ϕ for all phases that can form in a given alloy, it is possible to estimate equilibrium relative fractions of each phase and their constitution at a given temperature. This is performed by minimization of free energy curves of various phases. This procedure also allows for the determination of the tie line, which is schematically shown in Figure 3.

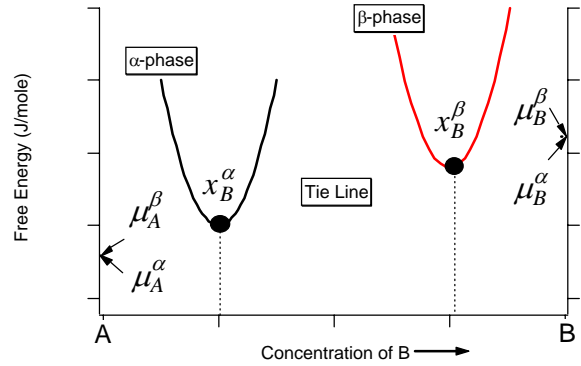


FIGURE 3. Free energy of a α -phase and β -phase and the common-tangent construction for the description of the tie line and chemical potential of elements A and B.

The chemical potential, μ_i^ϕ , of element i in ϕ -phase are obtained from the free energy expressions given in Equation 3 using the following relationship:

$$\mu_A^\phi = G^\phi - x_B^\phi \frac{\partial G^\phi}{\partial x_B^\phi}; \mu_B^\phi = G^\phi + (1 - x_B^\phi) \frac{\partial G^\phi}{\partial x_B^\phi} \quad (4)$$

Equations 3 and 4 can be extended to multicomponent systems by invoking the equality of chemical potential of other components. As an example, the equation governing equilibrium α and γ phases in the Fe-Cr-Ni-C alloy system is given below.

$$\mu_c^\gamma = \mu_c^\alpha; \mu_{\text{Fe}}^\gamma = \mu_{\text{Fe}}^\alpha; \mu_{\text{Cr}}^\gamma = \mu_{\text{Cr}}^\alpha; \mu_{\text{Ni}}^\gamma = \mu_{\text{Ni}}^\alpha; \quad (5)$$

Using the above relation, with appropriate mathematical methods, one can calculate the phase equilibrium between γ and α phases as a function of Cr, Ni and C concentration.

Although the phase stability calculation allows one to estimate the equilibrium microstructure at a particular temperature, microstructural control in most

thermal processes relies on the kinetics of product phase formation from the parent phase. For example, in low-alloy steels, it is important to understand the kinetics of austenite formation to control the microstructural mixture of ferrite and martensite in duplex steels. In addition to the kinetics of transformation, the equilibration of the non-equilibrium microstructure that is formed during processing is also of great interest. Both of the above phenomena can be described using diffusion controlled growth models. This can be achieved by coupling thermodynamic models and diffusion controlled growth calculations.

Formation of a product phase with a different composition from the parent phase involves diffusion of partitioning elements. By assuming that there exists a local-equilibrium between the parent and product phase at the interface, the interfacial concentrations can be given by the tie-lines drawn in the phase diagram. Given this condition, it is possible to describe the movement of this interface as a function of temperature and time by solving Fick's second law and maintaining the mass-balance at the interface. The governing equation for α -phase formation in γ -phase in one-dimension is given as an example below.

$$\left(C_I^{m,\alpha} - C_I^{m,\gamma}\right)(dl/dt) = D_\gamma^m \left(dC_\gamma^m/dx\right) - D_\alpha^m \left(dC_\alpha^m/dx\right) \quad (6)$$

In the above equation, (dl/dt) is the rate of interface movement or velocity. The terms $C_I^{m,\alpha}$ and $C_I^{m,\gamma}$ are the interface concentrations of element "m" in the α -phase and γ -phase. The terms D_α^m and D_γ^m are the diffusivity of element "m" in α -phase and γ -phase. The terms (dC_γ^m/dx) and (dC_α^m/dx) are the concentration gradient of element "m" in α -phase and γ -phase.

EXPERIMENTAL

Earlier experiments were conducted to validate the process and materials models. These initial results provided experimental data representing the thermal cycles experienced in the laser surface melt pool. This data was utilized for comparison to predicted thermal histories, as well as input for the computational thermodynamic and kinetic analyses. The material simulation techniques were then utilized to identify and corroborate material systems that would achieve beneficial coating characteristics using the laser surface modification process. This resulted in a selection of several hard particles, such as WC, TiC,

and TiN, and a cost-effective matrix material, representing the martensitic-grade, stainless steel alloy 431 being evaluated. It was also ascertained during materials simulations that shielding gas could be utilized to improve the chemical stability of these systems; hence, shielding gas was also incorporated into the evaluation.

Laser surface modification experiments were conducted using a Hobart Model HLP 3000 Nd:YAG laser system operating in a continuous-wave mode and providing 2430 W to the substrate. The beam was provided to the substrate at a 15-degree angle off of vertical. An f16 focus optic was used during processing, and resulted in a beam spot size at the work-piece of 5 mm. The beam energy distribution exiting the focusing optics was a "top hat" configuration. Shielding gas was supplied by a 5 mm inside diameter copper tube directed at the front of the pool at an angle of 30 degrees off of vertical. Shielding gas of Ar or a mixture of Ar and N₂ was utilized. A linear motion device was used to manipulate the beam to produce a scanning velocity of 2.12 mm s⁻¹.

Substrate material was 10.0 cm thick 1020 steel, and in all cases, the matrix material was Sulzer Metco 42C stainless steel alloy 431 powder having a size range of -325 to +80 mesh (44 to 177 μ m), and having a nominal composition of 16Cr, 1.9Ni, 1.0Si, 1.0 Mn, 0.20 C, and the balance being Fe. The hard particles used during these experiments were: AEE Corporation TiC powder having a purity of 99.9%, and believed to be in the -325 to +150 mesh (44 to 99 μ m) size range. Pre-placed powder was deposited on the substrate to a height of 2.0 mm prior to processing.

RESULTS AND DISCUSSION

The bead profiles and microstructures obtained during the laser modification experiments using stainless steel alloy 431 powder with and without TiC on a 1020 steel substrate are shown in Figures 4 and 5, respectively. The bead profiles were seen to change with processing conditions, and this is currently under additional analysis. The microstructure of the deposit produced using only alloy 431 powder and argon shielding gas did not contain any carbide and exhibited a martensite matrix. The microstructure of the deposit produced using alloy 431 with 20% TiC and argon shielding gas showed the presence of fine carbides having a particle morphology with some dendritic forms. The microstructure of the deposit produced using alloy 431 with 20-wt.% TiC and 90% argon and

10% N₂ shielding gas mixture exhibited remnants of original TiC provided the experiment.

The presence of fine particles smaller than the original particle size indicates that most of the original TiC powders dissolve in the liquid steel. On dissolution, the supersaturation of titanium and carbon increases, as well as the nitrogen, due to dissolution from the shielding environment. Then, during cooling from high temperature, the dissolved titanium, carbon, and nitrogen react to precipitate as titanium carbonitride [Ti(CN)]. The presence of dendritic shaped Ti(CN) particles indicates these precipitates are forming much before the primary solidification of iron matrix.

The microstructural evolution under argon and nitrogen shielding was further evaluated with phase stability calculations as a function of temperature using ThermoCalc® software with the ThermoTech-Iron database. It is important to note that TiCN and TiC are both equivalent and represented by a face-centered-cubic crystal structure in these calculations,

and the differentiation between TiC and TiCN are based only on the nitrogen content in the phase constitution. In the first case, the evolution of phases for an alloy composition given by 80-wt.% 431 martensitic steel and 20-wt.% TiC powder (Fe-4.17C-0.8Si-0.8Mn-12.8Cr-15.99Ti) was calculated. In the next case, the same alloy with 0.047-wt.% N was calculated. This value was based on the thermodynamic equilibrium calculation between pure liquid iron and atmospheric air at 2473 K and ignores the enhanced nitrogen dissolution due to the presence of monoatomic nitrogen in the plasma plume near the laser interaction zone. The calculated phase stabilities are shown in Figure 6. Stabilities of other phases such as FCC (austenite), BCC (ferrite), and M₂₃C₆, were similar for both steels. However, the calculations indicate that TiC will form from the liquid first for steel with no nitrogen and TiCN will form for steel with nitrogen. In the case of steel without nitrogen, TiC forms at 2357 K and the TiCN forms at 2396 K. The above results are in qualitative agreement with experimentally observed dendritic carbides observed in the optical microstructures.

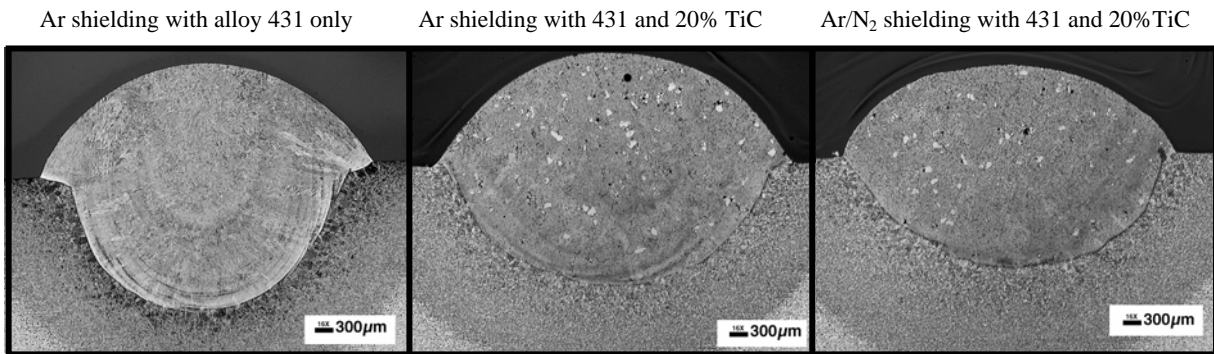


FIGURE 4. Macrographs of laser surface modification experiments with alloy 431 powder and TiC additions.

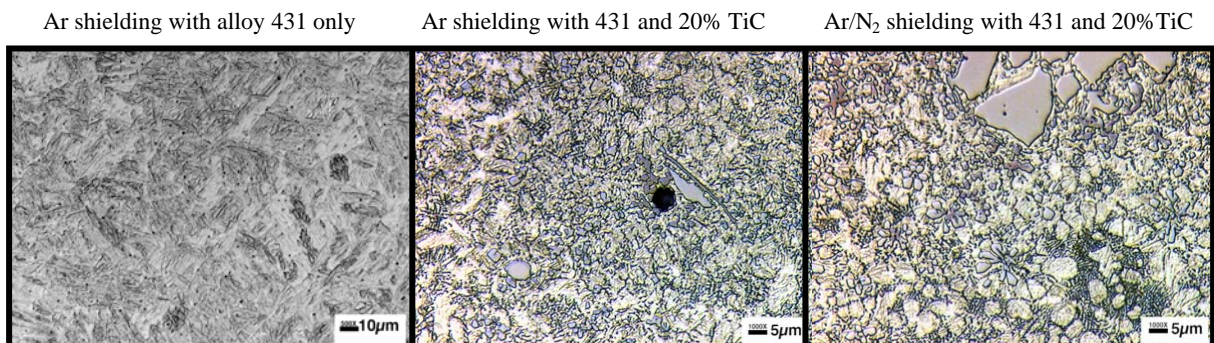


FIGURE 5. Micrographs of laser surface modification experiments with alloy 431 powder and TiC additions.

The average hardness of the laser surface modifications was also obtained. The deposit representing only the 431 alloy with argon shielding exhibited an average hardness of 438 HV. With the addition of 20% TiC to the 431 powder, an average hardness of 574 HV was observed. This increase in hardness is attributed to the addition of TiC to the deposit. The average hardness of the deposit produced using alloy 431 and 20% TiC with a mixture of Ar and N₂ was 621 HV, which is believed due to increasing levels of dissolved nitrogen, as well as the hard Ti(CN) compound that was expected to form by reaction with dissolved titanium and carbon.

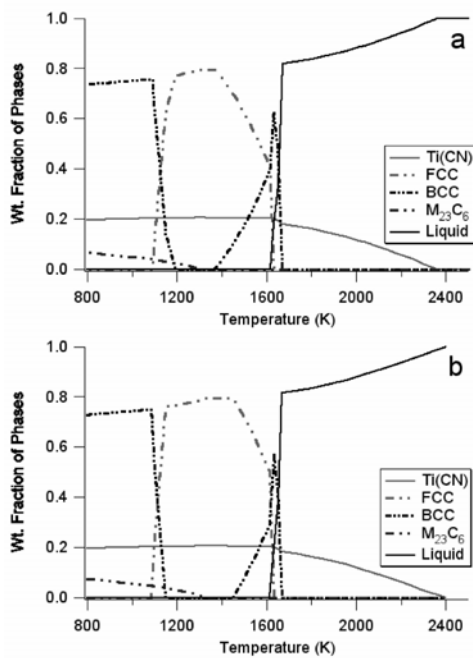


FIGURE 6. Comparison of calculated weight fraction of different phases in the laser surface layer deposit for two different compositions (a) Fe-4.17C-0.8Si-0.8Mn-12.8Cr-15.99Ti (wt.%) and (b) Fe-4.17C-0.8Si-0.8Mn-12.8Cr-15.99Ti-0.047N (wt.%).

CONCLUSIONS

The simulation and analysis techniques developed during this research is applicable to aiding and guiding materials selection and process parameters for achieving improved microstructures associated with the laser surface modification process. Laser deposits produced using alloy 431 and TiC powder with argon shielding resulted in microstructures retaining some TiC particles and an increase in hardness when

compared to deposits produced using only the 431 powder. Laser deposits representing alloy 431 and TiC powder and produced with a mixture of argon and nitrogen, as an active shielding gas, produced a further increase in hardness resulting from a microstructure retaining some TiC particles, as well as fine precipitates of Ti(CN) formed during cooling.

ACKNOWLEDGMENTS

Research at ORNL is sponsored by the U.S. Department of Energy, Office of Energy Efficiency and Renewable Energy, Industrial Technologies Program, Industrial Materials for the Future, under contract DE-AC05-00OR22725 with UT-Battelle, LLC. Research at Penn State University is sponsored by the Department of Energy's Industrial Materials for the Future Program under contract DE-FC07-02ID14247. The authors would also like to acknowledge the contributions of Mr. Shawn Kelly and Mr. Jay Tressler in the supporting various theoretical and experimental tasks described in this manuscript.

REFERENCES

1. Babu, S. S., Martukanitz, R. P., Parks, K. D., and David, S. A., *Met. And Mat. Trans. A*, Vol. 33A, 2002, p. 1189.
2. Zhu, S. M., Wang, L., Li, G. B., and Tjong, S. C., *Mat. And Eng. A*, L5, 1995, p. A201.
3. Colaco, R., Pino, C., and Vilar, R., *Scripta Mat.*, Vol. 41, 1997, p. 715.
4. Martukanitz, R. P., Unpublished Research, Applied Research Laboratory, Pennsylvania State University, 2000.
5. Pelletier, J. M., Oucherif, F., Sallamand, A. B. and Vannes, *Mater. Sci. Eng.*, Vol. A202, 1995, p. 142.
6. Ricciardi, G. Cantello, M., Molino, G., Varani, W., and Carlet, E., *Key Eng. Mater.*, Vol. 46, 1990, p. 415.
7. Dehm, G. Scheu, C., and Bamberger, M., *Proceedings of the Conference on Laser Materials Processing*, LIA, Vol. 2, 1997, p. 128.
8. Goldfarb, I. And Bamberger, M., *Scripta Mat.*, Vol. 34, 1996, p. 1051.
9. Carnahan, B., Luther, H.A., Wilkes, J.O., *Applied Numerical Methods*, John Wiley and Sons, Inc., New York, 1969, p. 431.
10. Batchelor, G.K., O'Brien, R.W., *Proceedings of the Royal Society of London, A-Mathematical and Physical Sciences*, Vol. 355, 1977, p. 313.

11. Babu, S. S., David, S. A., Vitek, J. M., Mundra, K., and DebRoy, T., *Sci. and Tech. of Weld. and Join.*, Vol. 4, 1999, p. 276.
12. Saunders, N. and Miodownik, A. P., *CALPHAD-Calculation of Phase Diagrams - A Comprehensive Guide*, Pergamon, Elsevier Science Inc, New York, 1998.